molecular pharmaceutics

ARTICLE

pubs.acs.org/molecularpharmaceutics

Blockade of Her2/*neu* Binding to Hsp90 by Emodin Azide Methyl Anthraquinone Derivative Induces Proteasomal Degradation of Her2/*neu*

Yan-yan Yan,[†] Li-sheng Zheng,[†] Xu Zhang,[‡] Li-kun Chen,[§] Satyakam Singh,[∥] Fang Wang,[†] Jian-ye Zhang,[†] Yong-ju Liang,[†] Chun-ling Dai,[†] Lian-quan Gu,[⊥] Mu-sheng Zeng,[†] Tanaji T. Talele,[∥] Zhe-sheng Chen,[∥] and Li-wu Fu*[,†]

[†]State Key Laboratory of Oncology in Southern China, Cancer Center, [‡]Department of Thorax, Cancer Center, [§]Department of Internal Medicine, Cancer Center, Sun Yat-sen University, Guangzhou, People's Republic of China

[∥]Department of Pharmaceutical Sciences, College of Pharmacy and Allied Health Professions, St. John's University, Queens, NY, USA

[⊥]Institute of Medicinal Chemistry, 132 East Circle at University City Guangzhou, Sun Yat-sen University, Guangzhou, People's Republic of China

Supporting Information

ABSTRACT: Overexpression of HER2/*neu*, a transmembrane tyrosine kinase acting as a coreceptor for other EGFR family members, is well-known to be associated with a poor prognosis in cancer. In the present study, we observed that emodin AMAD, a novel emodin azide methyl anthraquinone derivative, extracted from nature's giant knotweed rhizome of traditional Chinese herbs, potently decreased Her2/*neu* protein in dose- and time-dependent manners and also inhibited the downstream MAPK and PI3K-Akt signaling pathway. Intriguingly, reverse transcription-PCR and protein turnover assay revealed that the decrease of Her2/*neu* was independent of mRNA level but primarily owing to its protein stability. Meanwhile, proteasome inhibitor MG132 but not lysosome inhibitor chloroquine could restore Her2/*neu* and polyubiquitination of Her2/*neu* was augmented during emodin AMAD treatment. Furthermore, immunofluorescence study with anti-Her2/*neu* antibody showed that emodin AMAD disturbed the subcellular distribution of Her2/*neu*, with decreased location in the plasma membrane. Molecular docking studies predicted that AMAD can interact with the ATP-binding pocket of both Hsp90 and Her2/*neu*. Importantly, coimmunoprecipitation and immunofluorescence study revealed that emodin AMAD markedly impaired the binding between Hsp90 and Her2/*neu* and could bind to both Hsp90 and Her2/*neu* as reinforced by molecular modeling studies. In addition, combination of emodin AMAD treatment and siRNA against Her2 synergistically inhibited proliferation and induced apoptosis. Taken together, these data suggest that blockade of Her2/*neu* binding to Hsp90 and following proteasomal degradation of Her2/*neu* were involved in emodin AMAD-induced apoptosis in Her2/*neu*-overexpressing cancer cells. Our results provide suggestions that emodin AMAD could be promising as a new targeting therapeutic strategy in the treatment of Her2/*neu*-overexpressing cancers.

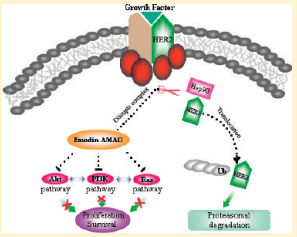

KEYWORDS: emodin AMAD, Her2/*neu*, heat shock protein 90, ubiquitin-proteasome, siRNA, docking

1. INTRODUCTION

Cancer has become an increasing public health problem for its high rates of morbidity and mortality. Recent data, including microarray results, have shown that Her2/*neu*-positive carcinomas represent a particular subset with distinct clinical and biological characteristics. Amplification of the Her2 gene has been reported in several types of cancer, including breast, ovarian, stomach, and NSCLC,[1−4] and most of these cases have been associated with poor prognosis.[5−7]

During the past decade, Her2/*neu* has been targeted for the development of novel anticancer drugs in the form of small molecules (e.g., lapatinib) or monoclonal antibodies (e.g., herceptin), and those have shown promising outcomes.[8,9] However, their efficacy and long-term application in patients are quite limited due to resistance and/or severe side effects, which necessitate the effort to develop novel therapeutic strategies.

The ubiquitin-proteasome pathway is essential for many fundamental cellular processes, including cell cycle, apoptosis, angiogenesis, and differentiation.[10] In addition, the proteasome contributes to the pathologic state of several human diseases including cancer and AIDS, in which some regulatory proteins are either stabilized due to decreased degradation or lost owing to accelerated degradation.[11] Therefore, targeting disease-associated proteins for ubiquitination and degradation represents a promising alternative therapeutic strategy in cancer.

Emodin AMAD (Figure 1A), belonging to emodin azide methyl anthraquinone derivative and obtained from structural modification of emodin extracted from nature's giant knotweed

Received: January 30, 2011
Accepted: August 3, 2011
Revised: July 11, 2011
Published: August 03, 2011

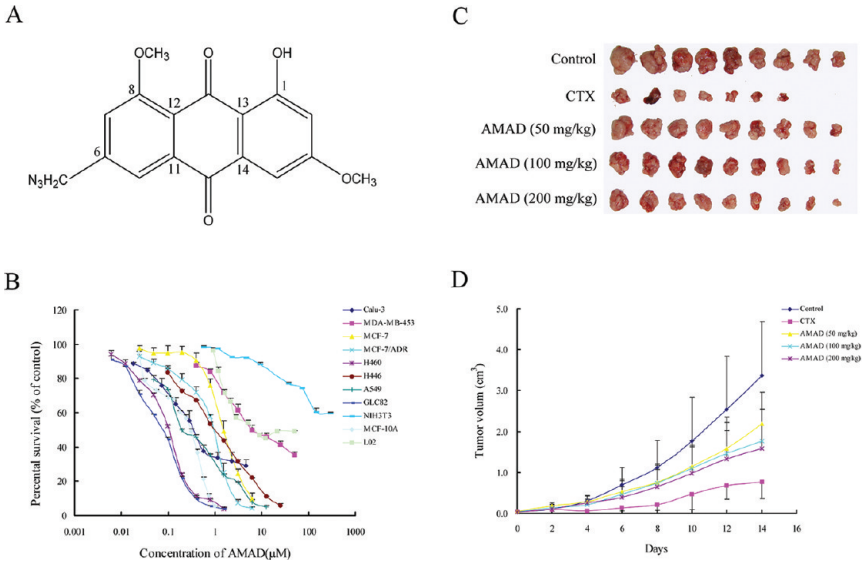

Figure 1. AMAD showed potent anticancer effect on breast cancer and lung adenocarcinoma cell lines *in vitro* and *in vivo*. (A) Chemical constitution of emodin AMAD. (B) AMAD showed cytotoxicity in diverse breast and lung adenocarcinoma cell lines. MCF-7, MCF-7/ADR, Calu-3, MDA-MB-453, A549, H446, H460, GLC82, NIH3T3, MCF-10A and L02 cells were treated with indicated concentrations of AMAD. Relative cell survival was determined 72 h after drug addition by the MTT assay. Points represent mean and bars represent SEM. Each point contained four duplication and three independent experiments were performed with one present. (C, D) AMAD suppressed the growth of H460 xenograft in nude mice.

rhizome of traditional Chinese herbs, has been demonstrated in our laboratory to trigger mitochondrial-dependent apoptosis in Her2/*neu*-overexpressing cancer cells.[12] However, multiple mechanisms are likely contributing to its anticancer activity. Thus, the present study was designed to further investigate the effects on Her2/*neu* of emodin AMAD *in vitro* and *in vivo* and the mechanisms involved.

2. EXPERIMENTAL SECTION

2.1. Chemicals and Reagents. Antibodies against Her2/*neu*, p-Her2/*neu*, FoxO1, p-FoxO1, mTOR, p-mTOR, p-GSK-3α/β, COX-2 and ubiquitin were obtained from Cell Signaling Technology (Danvers, MA). Antibodies against GSK-3α/β, Hsp70, HER1 and Hsp90 and immunoprecipitation reagent Protein A-Agarose Beads were purchased from Santa Cruz Biotechnology (Santa Cruz, CA). Antibodies against Akt, p-Akt (Ser473), ERK1/2, p-ERK1/2 and glyceraldehyde-3-phosphate dehydrogenase, anti-mouse and anti-rabbit IgG-horseradish peroxidase were purchased from Kangchen Biotechnology. (Shanghai, China). Anti-rabbit IgG-fluorescein isothiocyanate (FITC), anti-mouse IgG-FITC, anti-mouse IgG-Cy3, proteasome inhibitor MG132, lysosome inhibitor chloroquine, protein synthesis inhibitor cycloheximide and 3-(4,5-dimethylthiazol-2-y1)-2,5-diphenyltetrazolium bromide (MTT) were purchased from Sigma (St. Louis, MO). Hsp90 specific inhibitor 17-AAG was purchased from Multisciences biotechnology. (Hangzhou, China). Other routine laboratory reagents of analytical or high-performance liquid chromatography grade were obtained from Whiga Biotechnology (Guangzhou, China). Emodin AMAD with a purity of >98% was obtained from structural modification of emodin extracted from nature's giant knotweed rhizome of traditional Chinese herbs.[12] Cy7 labeled emodin AMAD (Cy7-AMAD) was synthesized by Fanbo Biochemicals Co., Ltd. (Beijing, China) with a purity of >87% (Supporting Information Figure S2).

2.2. Cell Lines and Culture. Human breast cancer cell lines MDA-MB-453, MCF-7, MCF-7/ADR, human lung adenocarcinoma cell lines Calu-3, A549, H446, H460, GLC82 and normal mouse fibroblast cell line NIH3T3 obtained from Cell Bank of Chinese Academy of Medical Sciences (Beijing, China) were cultured in DMEM, MEM/nonessential amino acid, and RPMI 1640, respectively, which containing 100 units/mL penicillin, 100 μg/mL streptomycin, and 10% fetal bovine serum. Normal human mammary epithelial MCF-10A cells were cultured in keratinocyte-SFM medium (Invitrogen, Grand Island, NY) supplemented with bovine pituitary extract. Normal human liver cell line L02, kindly provided by Professor Dan Xie, were cultured in DMEM containing 10% fetal bovine serum. All cells were cultured in a humidified atmosphere incubator(Forma 3111, Thermo Fisher Scientific Inc., Waltham, MA) containing 5% CO2 and 95% air at 37 °C.

2.3. Cell Viability Assay. Cells harvested during logarithmic growth phase were seeded in 96-well plates in a volume of 190 μL/well. After 24 h of incubation, 10 μL of AMAD full-range concentration was added to the 96-well plates. After 68 h of treatment, 10 μL of MTT (10 mg/mL stock solution of saline) was added to each well for 4 h. Subsequently, the supernatant was removed, and MTT crystals were solubilized with 100 μL of anhydrous DMSO in each well. Thereafter, cell viability was measured by model 550 microplate reader (Bio-Rad) at 540 nm with 655 nm as reference filter.[13] The 50% inhibitory concentration (IC_{50}) was determined as the anticancer drug concentration causing 50% reduction in cell viability and calculated from the cytotoxicity curves (Bliss's software). Cell percent survival rate was calculated using the following formula: survival (%) = (mean experimental absorbance/mean control absorbance) × 100%.

2.4. Establishment of Xenograft Model in Nude Mice. Athymic nude mice (BALB/c-nu-nu), male or female (5−6 weeks old, 24−26 g), were obtained from the Center of Experimental Animals, Sun Yat-sen University (Guangzhou, China). All animals were fed with sterilized food and water, and

experiments were carried out according to the Guidelines on Animal Care and Experiments of Laboratory Animals of the Center of Experimental Animals, Sun Yat-sen University, and approved by Ethics Committee for animal experiments. Human non-small cell lung carcinoma (NSCLC) H460 cell xenograft model was established as follows. In detail, transplantable H460 cells were harvested, suspended at a concentration of 10^7 cells/mL and implanted to mice for chemotherapeutic studies. Mice received a subcutaneous (sc) injection of 2×10^6 cells/inoculation under the right armpits. When mean diameter of tumors was approximately 0.5 cm, animals were randomized into five groups including control (normal saline 10 mL/kg), AMAD alone (50, 100, and 200 mg/kg), intraperitoneally (ip), q2d × 5 and cyclophosphamide (CTX) alone (100 mg/kg), i.p., q7d × 2. The weight of animals was measured every 2 days. When receiving the desired drug and dosage, each animal was tagged in the ear and followed individually throughout the experiment. We monitored tumor growth starting on the first day of treatment and measured the volume of the xenografts every 2 days. Tumor volume was measured in two perpendicular diameters (A and B). Tumor volume (V) was estimated according to the formula

$$V = \frac{\pi}{6}\left(\frac{A + B}{2}\right)^3$$

The curve of tumor growth was drawn according to tumor volume and treatment time. The mice were ethically killed when the mean tumor weight was over 1 g in the control group. Tumors were excised from the mice, and their weight was measured. The rate of inhibition (IR) was calculated according to the formula IR = 1 − (mean tumor weight of the experimental group/mean tumor weight of the control group) × 100%.

2.5. Immunoblotting. Cells were harvested and washed twice with ice-cold PBS, and the pellets were collected in 1× lysis buffer [50 mmol/L Tris-HCl (pH 6.8), 10% glycerol, 2% SDS, 0.25‰ bromophenol blue, and 0.1 mol/L DTT] was added for 100 μL/5 × 10^6 cells. After heated at 95 °C for 20 min, the lysates were centrifuged at 12,000 rpm for 10 min and the supernatant was collected. The protein concentration was determined by nucleic acid−protein analyzer (Beckman). Equal amount of lysate protein was separated on 8% to 12% SDS−PAGE and transferred onto polyvinylidene difluoride membrane (Pall). The nonspecific binding sites were blocked with TBST buffer containing 5% nonfat dry milk for 2 h at room temperature. The membranes were incubated overnight at 4 °C with specific primary antibodies, and the membranes were then washed thrice with TBST buffer and incubated at room temperature for 1 h with horseradish peroxidase-conjugated secondary antibody. After three washes with TBST buffer, the immunoblots were visualized by the enhanced Phototope-Horseradish Peroxidase Detection Kit purchased from Cell Signaling Technology and exposed to Kodak medical X-ray processor (Kodak, Rochester, NY).[12]

2.6. Immunoprecipitation. After exposure, whole cells were harvested and washed twice with ice-cold PBS, and the pellets were vortexed and 1× lysis buffer [20 mmol/L Tris (pH 7.5), 150 mmol/L NaCl, 1 mmol/L EDTA, 1 mmol/L EGTA, 1% Triton X-100, 2.5 mmol/L sodium pyrophosphate, 1 mmol/L β-glycerophosphate, 1 mmol/L Na_3VO_4, 1 μg/mL leupeptin] was added for 100 μL/5 × 10^6 cells. Cell lysates containing 1 to 1.5 mg total proteins were incubated with anti-Hsp90 or anti-Her2/*neu* antibody with gentle rocking overnight at 4 °C, followed by Protein A-Agarose Beads (20 μL of 50% bead slurry) for 3 h at 4 °C. The pellets were washed five times with 500 μL of 1× cell lysis buffer and resuspended with 20 μL of 3× SDS loading buffer. The samples were then heated and analyzed by Western blot.

2.7. Immunofluorescence Assay. After Calu-3 cells grown on coverslips were treated with 3.00 μmol/L AMAD for 48 h, cells were fixed with 4% polyoxymethylene for 20 min, and Triton X-100 was added for 10 min at room temperature. Then, the cells were rinsed with PBS three times, and the nonspecific binding sites were blocked in PBS with 1% bovine serum albumin for 1 h. The cells were incubated overnight at 4 °C with Her2/*neu* antibody followed by FITC-conjugated secondary antibody at room temperature for 1 h. Subcellular distribution of Her2/*neu* protein was observed under fluorescence microscopy with standard excitation filters (Leica Dmirb) in random microscopic field at ×400 magnification.[14]

2.8. Semiquantitative Reverse Transcription-PCR. Total cellular RNA was prepared using the TRIzol reagent (Invitrogen), and the first strand cDNA was synthesized by Oligo dT primers with reverse transcriptase (Promega, Madison, WI)). Using the GeneAmp PCR system 9700 (PE Applied Biosystems, Foster City, CA), reactions were carried out as following: GAPDH, at 94 °C for 3 min for initial denaturation, and then at 94 °C for 30 s, 55 °C for 30 s, and 72 °C for 1 min, after 30 cycles of amplification, additional extensions were carried out at 72 °C for 10 min; Her2, at 94 °C for 2 min for initial denaturation, and then at 94 °C for 30 s, 58 °C for 30 s, and 72 °C for 1 min for 10 cycles, at 93 °C for 30 s, 54 °C for 30 s, and 72 °C for 1 min for 20 cycles, after 32 cycles of amplification, additional extensions were also carried out at 72 °C for 10 min. Equal volumes of RT-PCR products were electrophoresed on 0.8% agarose gel stained with 1.5 μmol/L ethidium bromide. Photography and analyses were performed with the gel imaging and analysis system (Vilber Lourmat, Marnela-Vallée, France). The primer sequences are as follows: Her2 forward, 5′-CTTCAAAGGGACACCTACGG-3′; Her2 reverse, 5′-CAGCCATCTGGGAACTCAA-3′; GAPDH forward, 5′-CTTTGGTATCGTGGAAGGA-3′; GAPDH reverse, 5′-CACCCTGTTGCTGTAGCC-3′. Expected PCR products were 233 bp for Her2 and 472 bp for GAPDH, respectively.

2.9. Protein Turnover Assay. After MDA-MB-453 and Calu-3 cells were treated with AMAD or DMSO for 12 h, the protein synthesis inhibitor cycloheximide (CHX, 10 μg/mL) was added to the cells. After treatment for additional indicated time, the whole cells were harvested at different time points and whole cell lysates were analyzed by Western blot.

2.10. RNA Interference. Calu-3 cells were harvested during logarithmic growth phase and inoculated in 6-well plates overnight to adhere. RNA interference was performed when the fusion rate was up to 30−50%. One day before the interference experiment, the cells were exposed to fresh medium with no antibiotic but fetal bovine serum. The siRNA sequences were synthesized by Shanghai GenePharma Biotechnology (Shanghai, China) and resolved in a concentration of 20 μmol/L. Before interference, each well was replaced with 900 μL of fresh medium without antibiotic and fetal bovine serum. 2 μL of Lipofectamine 2000 (Invitrigen) and 2.5 μL of siRNA solution were diluted in 48 and 47.5 μL of OPTIMEM I medium (Invitrogen), respectively, and were then incubated at room temperature for 5 min. Subsequently the two solutions were mixed and incubated at room temperature for 20 min before addition to the well. After

6 h of incubation, the cells were observed under fluorescence microscopy with standard excitation filters (Leica Dmirb) in random microscopic field (negative control FAM as a control for efficiency of transfection). Thereafter, the wells were charged with fresh medium with antibiotic and fetal bovine serum.[15] 48 h later, the cells were used for other assays. The siRNA sequences are as follows: Her2-I (741), sense 5′-CGUUUGAGUCCAUGCCCAATT-3′, antisense 5′-UUGGGCAUGGACUCAAACGTG-3′; Her2-II (1734), sense 5′-CCUACAUGCCCAUCUGGAATT-3′, antisense 5′-UUCCAGAUGGGCAUGUAGGAG-3′; Her2-III (2200), sense 5′-CAAAGAAAUCUUAGACGAATT-3′, antisense 5′-UUCGUCUAAGAUUUCUUUGTT-3′; Her2-IV (2515), sense 5′-GCUGGACAUUGACGAGACATT-3′, antisense 5′-UGUCUCGUCAAUGUCCAGCAG-3′; negative control and FAM negative control, sense 5′-UUCUCCGAACGUGUCACGUTT-3′, antisense 5′-ACGUGACACGUUCGGAGAATT-3′.

2.11. Annexin V/PI Double-Staining Assay. Annexin V and PI double-staining was performed using ApopNexin FITC Apoptosis Detection Kit (Millipore, Billerica, MA). 6×10^5 cells were seeded in 25 cm^2 flasks and allowed to attach for 24 h. After treatment with the desired concentrations of AMAD for 48 h, both floating and attached cells were collected, washed twice with ice-cold PBS and resuspended in 200 μL of 1× binding buffer containing Annexin V (1:50 solution according to the manufacturer's instruction) and 40 ng/sample PI for 15 min at 37 °C in the dark. Then the numbers of viable, apoptotic and necrotic cells were quantified by flow cytometer (Becton Dickinson) and analysis by the CellQuest software. Cells were excited at 488 nm, and the emission of Annexin V was at 525 nm, and PI was collected through a 610 nm band-pass filter. At least 10,000 cells were analyzed for each sample. The percent apoptosis (%) = (number of apoptotic cells/number of total cells observed) × 100%.

2.12. Molecular Modeling. Emodin AMAD was built using the fragment dictionary of Maestro 9.0 and energy minimized by Macromodel program v9.7 (Schrödinger, Inc., New York, NY, 2009) using the OPLSAA force field with the steepest descent followed by truncated Newton conjugate gradient protocol. Partial atomic charges were computed using the OPLS-AA force field. The low-energy 3D structures of emodin AMAD were generated with the following parameters present in LigPrep v2.3: different protonation states at physiological pH, all possible tautomers and ring conformations.

The X-ray cocrystal structures of Her2-SYR127063 (PDB ID: 3PP0)[16] and HSP90-ADP (PDB ID: 1BYQ)[17] obtained from the RCSB Protein Data Bank were used for docking into active sites of Her2 and HSP90, respectively. The initial structure thus obtained was refined by means of default parameters mentioned in protein preparation tool implemented in Maestro v9.0 and Impact program v5.5 (Schrödinger, Inc., New York, NY, 2009), in which the protonation states of residues were adjusted to the dominant ionic forms at pH 7.4. Refined Her2 and HSP90 models were further used to generate receptor grid by selecting bound SYR127063 and ADP ligands, respectively.

Emodin AMAD was docked within the nucleotide binding sites of Her2 and HSP90 using the "Extra Precision" (XP) Glide docking program v5.5 (Schrödinger, Inc., New York, NY, 2009) and the default parameters. The top scoring pose of emodin AMAD within the active sites of both proteins was then subjected to energy minimization using Macromodel program v9.7 and used for graphical analysis. All computations were carried out on a Dell Precision 470n dual processor with the Linux OS (Red Hat Enterprise WS 4.0).

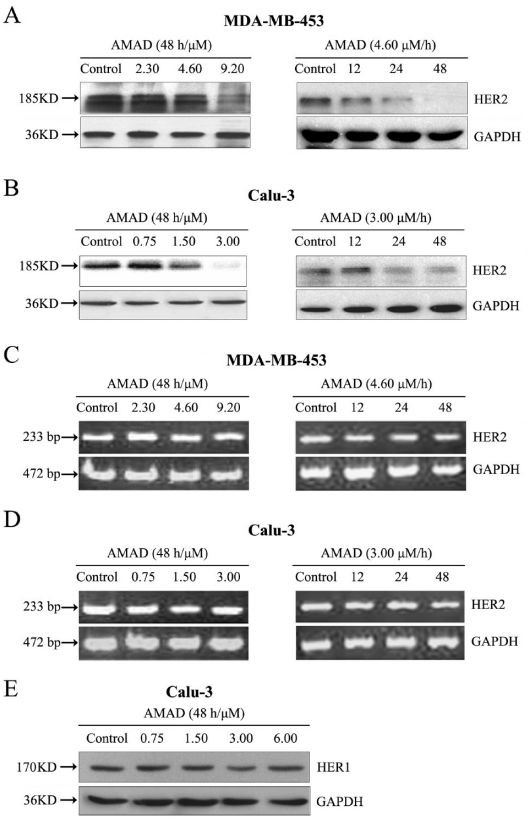

Figure 2. AMAD downregulated Her2/*neu* independent of its mRNA level. (A, B) AMAD downregulated Her2/*neu* protein in dose- and time-dependent manners. After MDA-MB-453 and Calu-3 cells were exposed to indicated concentrations of AMAD for the indicated time, the whole-cell lysates were assayed by Western blot. (C, D) AMAD did not affect Her2 mRNA expression. After AMAD treatment, total cellular RNA was prepared, and RT-PCR analysis was performed as described in the Experimental Section. (E) AMAD did not affect the protein expression of Her1.

2.13. Statistical Analysis. For each protocol, three independent experiments were performed. Results were expressed as the mean ± standard error of the mean (SEM). Statistical calculations were performed by using SPSS16.0 software. Differences in measured variables between experimental and control groups were assessed by Student's *t*-test. **, $p < 0.01$ was indicative of very significant difference.

3. RESULTS

3.1. AMAD Showed Potent Anticancer Effect on Breast Cancer and Lung Adenocarcinoma Cell Lines *in Vitro* and *in Vivo*. As shown in Figure 1B and Supporting Information Table S1, AMAD exerted potent cytotoxic effect on diverse breast cancer and lung adenocarcinoma cell lines, with the IC_{50} values ranging from 0.18 to 9.06 μmol/L, including Her2/*neu*-overexpressing MDA-MB-453 and Calu-3 cells. Intriguingly, AMAD showed no cytotoxic effect on normal mouse fibroblast NIH3T3 cells; however, it showed some cytotoxicity on normal human mammary epithelial MCF-10A cells and normal human liver cell line L02. Other mechanisms may be involved in its cytotoxicity on low Her2/*neu*-expression cells. In the nude mice xenograft model, AMAD significantly inhibited the growth of H460 xenograft in a dose-dependent manner, with no significant body

weight loss and other severe side effects (Figure 1C,D, Supporting Information Table S2). After administration of 200 mg/kg AMAD for 14 days, the growth of H460 xenograft was inhibited by up to 50.7%.

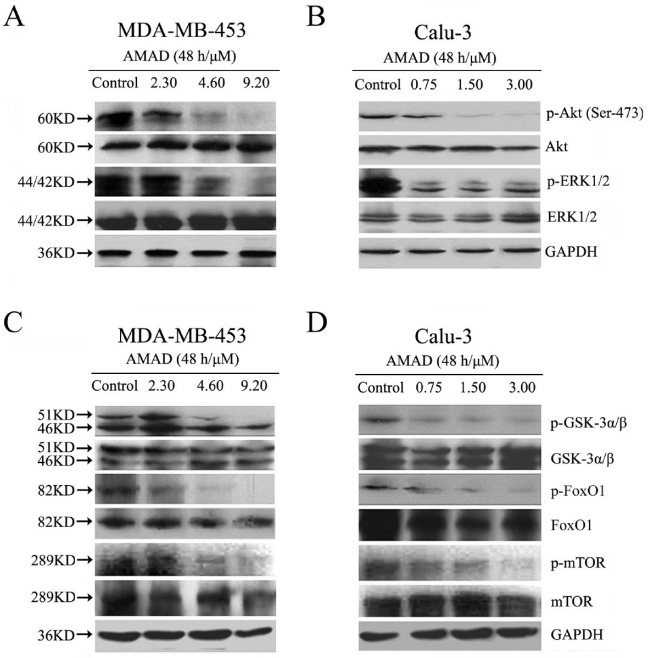

Figure 3. AMAD inhibited downstream signaling pathways of Her2/*neu*. After treatment with the indicated concentrations of AMAD for 48 h, the whole-cell lysates of MDA-MB-453 and Calu-3 cells were assayed by Western blot. (A, B) AMAD suppressed phosphorylation of Her2/*neu* downstream ERK and Akt. (C, D) AMAD repressed Akt downstream signaling events.

3.2. AMAD Downregulated Her2/*neu* Protein Expression and Inhibited Downstream Signaling Pathways in Her2/*neu*-Overexpressing Cancer Cells. Her2/*neu*-overexpressing cancer cells have been shown to activate downstream MAPK (mitogen-activated protein kinase) and PI3K (phosphatidylinositol 3-kinase)/Akt signaling pathway. As shown in Figure 2A, B,E, AMAD significantly downregulated Her2/*neu* protein expression in dose- and time-dependent manners in both MDA-MB-453 and Calu-3 cells, without changing the expression of Her1 protein. Furthermore, AMAD had no effect on total Akt and ERK1/2 proteins, whereas p-Akt (Ser473) and p-ERK1/2 were inhibited in a dose-dependent manner (Figure 3A,B).

Akt kinase has been shown to phosphorylate several key substrates that regulate protein translation, apoptosis, and cellular proliferation.[18,19] Our data showed that AMAD inhibited the phosphorylation of GSK-3α/β, FoxO1 and mTOR which could be phosphorylatd by Akt at concentrations associated with inhibition of Akt activation (Figure 3C,D).

3.3. Downregulation of Her2/*neu* by AMAD Was Primarily Dependent on Her2/*neu* Protein Stability. To examine whether Her2/*neu* was downregulated by AMAD at the mRNA level, we analyzed Her2 mRNA expression by semiquantitative RT-PCR. As shown in Figure 2C,D, after MDA-MB-453 and Calu-3 cells were exposed to AMAD, no significant change in Her2 mRNA expression was observed.

Like several other membrane proteins, the level of Her2/*neu* seems to be regulated by protein stability.[20−22] To investigate whether AMAD could downregulate Her2/*neu* through this mechanism, the Her2/*neu* stability in MDA-MB-453 and Calu-3 cells was examined by protein turnover assay. The data revealed a half-life of 30.1 h for Her2/*neu* in MDA-MB-453 cells, which was significantly reduced to 7.3 h by AMAD (Figure 4A,C). Similarly, in Calu-3 cells, the half-life of Her2/*neu* was 54.1 h, which was also significantly decreased to 20.4 h by AMAD treatment (Figure 4B,D).

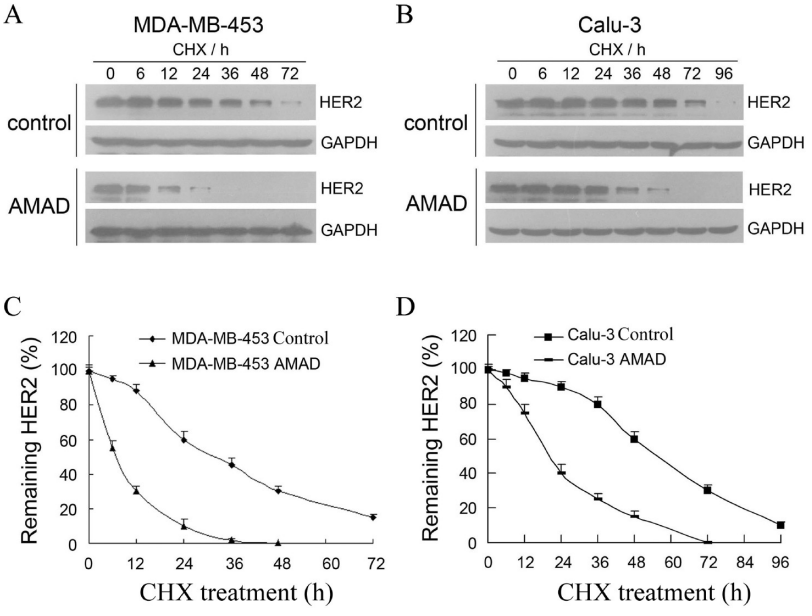

Figure 4. AMAD augmented the instability of Her2/*neu* protein. (A, C) AMAD decreased Her2/*neu* over time in MDA-MB-453 cells. After preincubation with 4.60 μmol/L AMAD or control (DMSO) for 12 h, cells were treated with the protein synthesis inhibitor cycloheximide (CHX, 10 μg/mL) for the indicated time. The protein level of Her2/*neu* was detected by Western blot (A), and quantification of remaining Her2/*neu* at different time points was represent as percent of initial Her2/*neu* at 0 h of CHX treatment (C). (B, D) Decrease of Her2/*neu* over time in Calu-3 cells. The concentration of AMAD was 3.00 μmol/L, and experiments and quantifications were performed as in MDA-MB-453 cells.

dx.doi.org/10.1021/mp2000499 |*Mol. Pharmaceutics* 2011, 8, 1687–1697

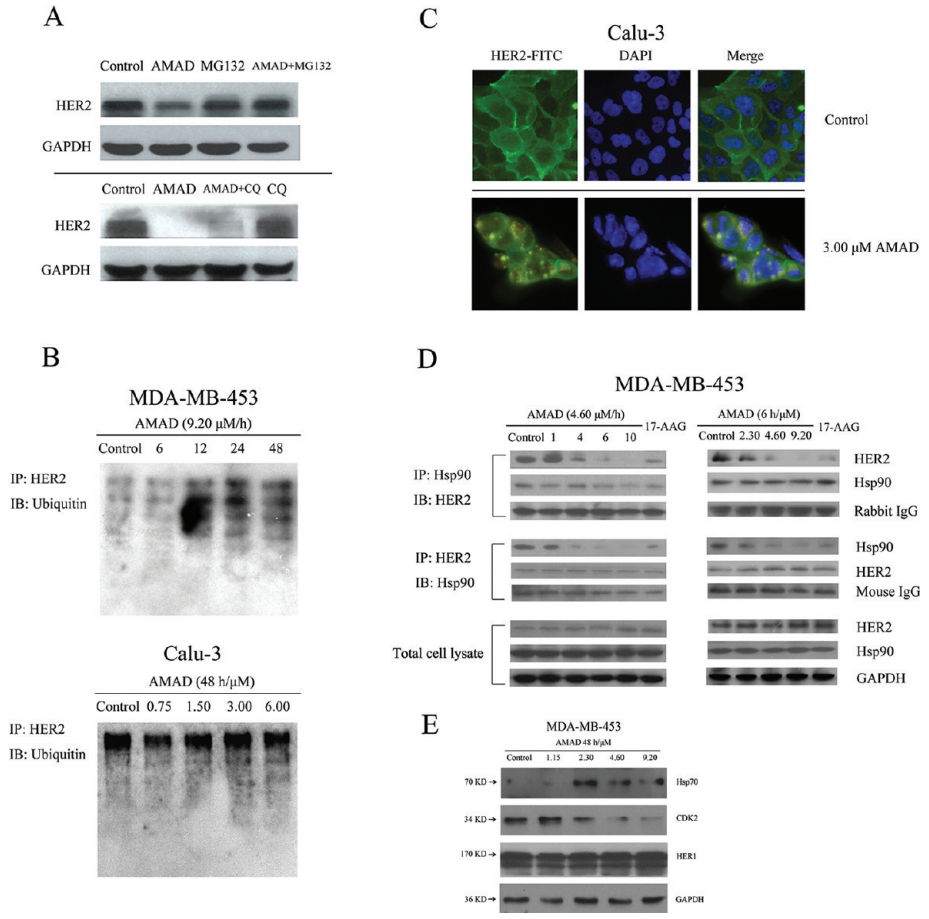

Figure 5. AMAD blocked Her2/*neu* binding of Hsp90 and promoted its degradation through the ubiquitin-proteasome pathway. (A) Proteasome inhibitor MG132 but not lysosome inhibitor chloroquine (CQ) restored Her2/*neu* after AMAD treatment. Calu-3 cells were treated with DMSO; 3.00 μmol/L AMAD for 48 h; 50 μmol/L MG132 or 50 μmol/L CQ for 60 h; or 50 μmol/L MG132 or 50 μmol/L CQ preincubation for 12 h followed by 3.00 μmol/L AMAD for 48 h. Her2/*neu* protein in whole-cell lysates was detected by Western blot. (B) AMAD induced polyubiquitination of Her2/*neu*. After MDA-MB-453 and Calu-3 cells were treated with the indicated time or concentrations of AMAD, Her2/*neu* protein was immunoprecipitated as described in the Experimental Section and analyzed for ubiquitination with anti-ubiquitin antibody by Western blot. (C) AMAD altered the subcellular distribution of Her2/*neu*. After Calu-3 cells grown on coverslips were treated with AMAD or DMSO for 48 h, immunofluorescence assay was performed according to the Experimental Section. (D) AMAD impaired the binding of Her2/*neu* and Hsp90. After MDA-MB-453 cells were treated with 4.60 μmol/L AMAD for the indicated time or indicated concentrations of AMAD for 6 h, coimmunoprecipitation was performed using anti-Hsp90 or anti-Her2/*neu* antibody as described in the Experimental Section, and rabbit and mouse IgG were used as loading controls, respectively. 17-AAG (2 μmol/L) for 24 h was used as a positive control. The levels of Hsp90 and Her2/*neu* in the total cell lysate were blotted as controls. (E) Changes of other Hsp90 client proteins after AMAD treatment in MDA-MB-453 cells. After MDA-MB-453 cells were treated with 1.15−9.20 μmol/L AMAD for 48 h, the whole-cell lysates were assayed by Western blot and corresponding antibodies.

3.4. AMAD Inhibited Her2/*neu* Binding to Hsp90 and Depleted Her2/*neu* by Proteasomal Degradation. As the central component of a ubiquitous chaperone complex, Hsp90 interacts with a variety of intracellular client proteins to facilitate their proper folding, prevent misfolding or aggregation, and preserve their 3-dimensional conformation to a functionally competent state.[23] Her2/*neu* has been demonstrated to be one of the client proteins of Hsp90.[24,25] To examine whether instability of Her2/*neu* protein induced by AMAD was due to the inhibition of binding between Hsp90 and Her2/*neu*, coimmunoprecipitation was performed. As shown in Figure 5D, after MDA-MB-453 cells were treated with 4.60 μmol/L AMAD for the indicated time or indicated concentrations of AMAD for 6 h, the binding of Her2/*neu* and Hsp90 was significantly inhibited.

Her2/*neu* protein has been demonstrated to be degraded in the proteasome by the antibiotic benzoquinone ansamycin.[26] Thus, we examined whether AMAD-induced depletion of Her2/*neu* also occurred through the proteasome pathway. Our data showed that pretreatment of Calu-3 cells with the proteasome inhibitor MG132 blocked the depletion of Her2/*neu* protein by AMAD, whereas pretreatment with the lysosome inhibitor chloroquine (CQ), on the other hand, had no such effect (Figure 5A). Meanwhile, AMAD augmented the polyubiquitinylation of Her2/*neu* (Figure 5B).

Immunofluorescence study with anti-Her2/*neu* antibody was also performed. As shown in Figure 5C, the control cells had strong immunofluorescence at the plasma membrane. After AMAD treatment, the immunofluorescence at the plasma membrane was attenuated and replaced with diffuse cytoplasmic and nuclear punctate staining. We also found that AMAD treatment and siRNA against Her2 significantly depleted Her2/*neu* protein, as well as a specific Hsp90 inhibitor

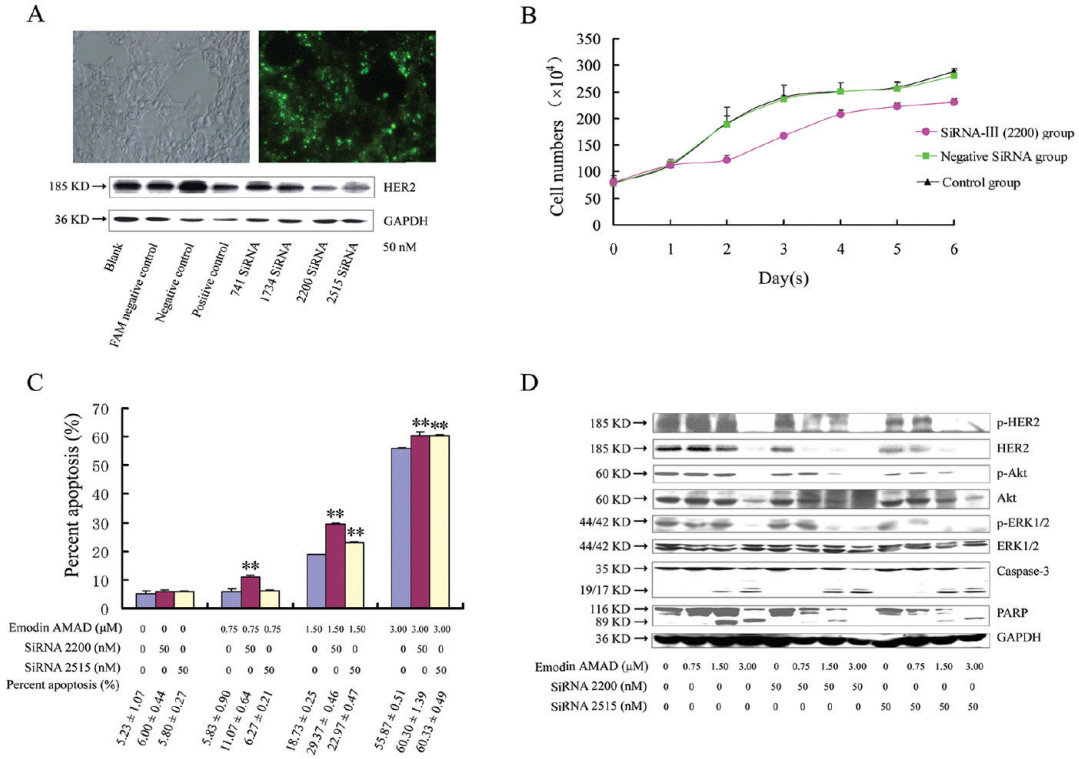

Figure 6. Combination of AMAD and siRNA against Her2 synergistically inhibited proliferation and induced apoptosis. (A) siRNA against Her2 decreased its protein level in Calu-3 cells. RNA interference was performed as described in the Experimental Section. Top, transfection of FAM negative control represent the efficiency of transfection. Bottom, Western blot analysis of Her2/*neu* protein represented the interference effectiveness of different siRNA sequences. siRNA against GAPDH was used as positive control. (B) siRNA of Her2 inhibited proliferation of Calu-3 cells. (C) Combination of AMAD and siRNA against Her2 more markedly induced apoptosis than AMAD alone in Calu-3 cells. The apoptosis rate of Calu-3 cells was detected and calculated as described in the Experimental Section by Annexin V/PI double-staining assay. **, $P < 0.01$ versus AMAD alone at each concentration. (D) Combination of AMAD and siRNA against Her2 further promoted Her2/*neu* protein degradation, inhibited downstream signaling pathways and induced apoptosis in Calu-3 cells by Western blot.

17-AAG, resulting decreased colocalization of Her2/*neu* and Hsp90 in Calu-3 cells (Supporting Information Figure S1A).

3.5. Combination of AMAD and siRNA against Her2 Synergistically Inhibited Proliferation and Induced Apoptosis. As shown in Figure 6A, the transfection efficiency of siRNA to target Calu-3 cells was significantly high and the sequence siRNA III (2200) and siRNA IV (2515) exerted the most potent effect on silencing Her2/*neu* expression revealed by Western blot analysis. Further investigation using siRNA III (2200) revealed that interference of Her2 by siRNA significantly inhibited the proliferation of Calu-3 cells (Figure 6B), and augmented the effect of AMAD on inducing apoptosis of Calu-3 cells (Figure 6C). Furthermore, combination of AMAD and Her2 siRNA further inhibited the phosphorylation of Her2/*neu*, ERK, Akt and induced the activation of Caspase-3 and PARP (Figure 6D).

3.6. Binding Mode of AMAD to Her2 and HSP90. The binding mode of AMAD within the nucleotide binding site of Her2 (Glide docking score = −6.65 kcal/mol) is shown in Figure 7A. The tricyclic aromatic ring structure of AMAD is extensively stabilized by hydrophobic residues Leu726, Val734, Ala751, Met801 and Leu852. The terminal negatively charged nitrogen (N_3) atom of the methyl-azide group is positioned to form an electrostatic interaction with the ε-NH_2 function of Lys724 (3.5 Å). The ε-NH_2 group of Lys753 and the carboxylate group of Asp863 are involved in a salt bridge interaction (conserved across all kinases) and help coordinate the α and β phosphates of ATP bound in the active site, a feature responsible for active conformation of the kinase. It may be noted that the oxygen atom of the hydroxyl group on the C-ring is located within hydrogen bond forming distance from the ε-NH_2 group of Lys753 and may compete with Asp863 for hydrogen bonding to Lys753 and eventually may lead to disruption of this crucial salt bridge interaction. The hydrogen atom of this hydroxyl group forms an intramolecular hydrogen bond with the B-ring carbonyl oxygen atom and provides conformational rigidity through a pseudo-six-membered ring, which may be advantageous due to the decreased number of degrees of freedom. The ether oxygen atom on the A-ring is located within hydrogen bonding distance from HOH155 (O···HOH155, 2.3 Å), which in turn is involved in a hydrogen bonding interaction with the side chain of Cys805, the target for irreversible tyrosine kinase inhibitors, (HOH···HS-Cys805) and HOH129 (HOH129···HOH155). The HOH129 forms a hydrogen bond with the backbone of Leu726. Thus, the azide, hydroxyl, ether and carbonyl groups on the anthracene ring system play an important role in stabilizing AMAD through electrostatic interactions, which may explain the significant loss of kinase activity upon modifications at the carbonyl groups on the B-ring, ether group on the A- and C-rings and hydroxyl function on the C-ring.[27]

Binding model of AMAD within the N-terminal ATP-binding pocket of HSP90 (Glide docking score = −5.98 kcal/mol) is shown in Figure 7B. Whereas the tricyclic aromatic ring structure of AMAD is stabilized by extensive hydrophobic interactions, its

dx.doi.org/10.1021/mp2000499 |*Mol. Pharmaceutics* 2011, 8, 1687–1697

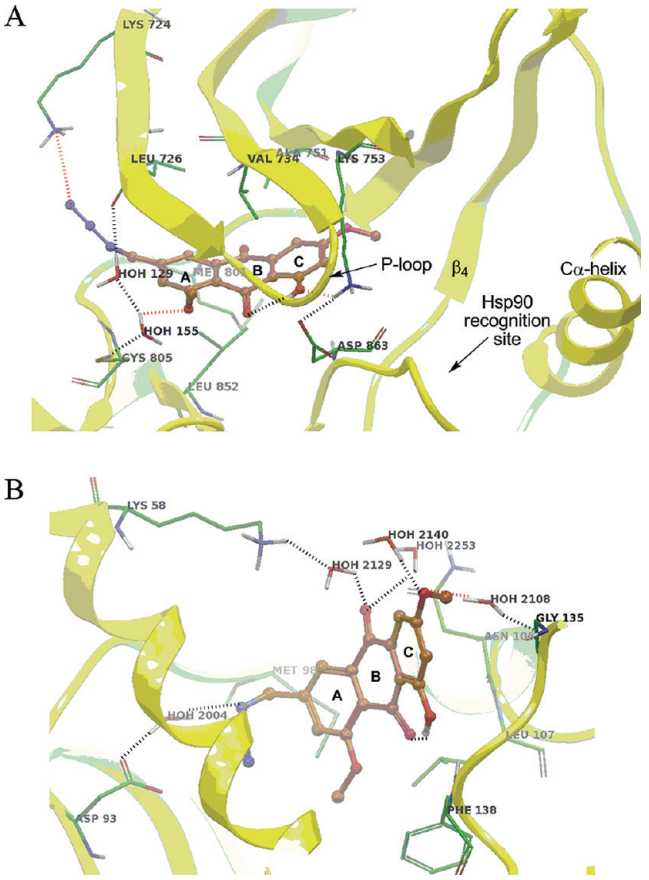

Figure 7. Glide predicted binding mode of AMAD within the nucleotide binding sites of Her2 (panel A) and HSP90 (panel B). Important amino acids and water molecules are depicted as sticks with the atoms colored as follows: carbon, green; hydrogen, white; nitrogen, blue; oxygen, red; and sulfur, yellow) whereas the inhibitor is shown as a ball and stick model with the same color scheme as above except carbon atoms are represented in orange color. Dotted black lines indicate hydrogen bonding interactions whereas dotted red lines indicate potential electrostatic interactions.

carbonyl, hydroxyl, ether and azide groups form an extensive water-mediated hydrogen bonding network within the nucleotide binding pocket. The hydrophobic interactions are mainly formed by residues Met98, Leu107 and Phe138. Another significant interaction comes from a network of water-mediated hydrogen bonding and electrostatic interactions. For example, the N_1 atom of the azide group forms a water-mediated hydrogen bonding interaction with the carboxylate group of Asp93 (azide $N_1\cdots$HOH2004, 2.2 Å; HOH2004$\cdots$O═C(O)-Asp93, 1.7 Å). One of the carbonyl oxygen atoms of the B-ring forms a water-mediated hydrogen bonding interaction with the ε-NH_2 function of Lys58 (C═O$\cdots$HOH2129, 2.1 Å; HOH2129$\cdots$ H_2N-Lys58, 2.0 Å). The same carbonyl oxygen atom also formed a second hydrogen bond with HOH2253, which in turn is located within hydrogen bonding distance from the side chain amide group of Asn106. The second carbonyl oxygen atom of the B-ring enters into an intramolecular hydrogen bonding interaction with the hydroxyl group of C-ring, thus forming a pseudo-six-membered-ring which may restrict loss of entropy. The ether oxygen atom on the C-ring forms a hydrogen bond with HOH2140. This ether oxygen atom is placed in the right geometry to form a second hydrogen bond with HOH2108 (2.1 Å, 150°), which in turn is involved in a hydrogen bonding interaction with the backbone of Gly135. It can be summarized that the carbonyl, hydroxyl, ether and azide functional groups on the anthracene ring structure are densely surrounded by active site water molecules (only representative ones are displayed for clarity), a characteristic of the N-terminal ATP-binding pocket of HSP90.

4. DISCUSSION

Like doxorubicin and daunorubicin, emodin (1,3,8-trihydroxy-6-methylanthraquinone) is a single anthracycline 1,8-dihydroxyanthraquinone derivative and is an active ingredient of various Chinese herbs including *Rheum officinale*, *Polygonum cuspidatum*, etc. As a tyrosine kinase inhibitor, emodin was found to block phosphorylation of Her2/*neu*, suppress growth, transformation and metastasis, induce differentiation and increase the susceptibility of Her2/*neu*-overexpressing cancer cells to standard cytotoxic therapeutic agents.[27−31] These indicated that emodin was probably a promising anticancer drug. However, compared with other monomers such as paclitaxel and camptothecin, the anticancer activity of emodin was not obvious and its side effects such as cardiac toxicity limited its clinical application in tumor chemotherapy, making the structural modification of emodin necessary.

Emodin AMAD, an emodin azide methyl anthraquinone derivative, has been demonstrated in our laboratory to induce mitochondrion-dependent apoptosis in Her2/*neu*-overexpressing MDA-MB-453 and Calu-3 cells.[12] Here, we showed that AMAD exerted potent cytotoxic effect on diverse breast cancer and lung adenocarcinoma cell lines, without obvious effect on NIH3T3 cells. Besides, AMAD significantly inhibited the growth of H460 xenograft in nude mice in a dose-dependent manner, with no significant body weight loss and other severe side effects (Figure 1, Supporting Information Tables S1 and S2). These suggested that AMAD may be as a promising candidate for cancer chemotherapy.

Her2/*neu* overexpression in cancers signifies poorer prognosis, yet it has provided a promising avenue for targeted therapy as demonstrated by the success of the humanized monoclonal antibody trastuzumab (e.g., herceptin) and small molecule tyrosine kinase inhibitors (e.g., lapatinib). Resistance, severe side effects, eventual failure in most cases and expensive cost, however, necessitated alternate Her2/*neu*-targeted therapies.[32] Here, we observed that AMAD achieved effective downregulation of Her2/*neu* in dose- and time-dependent manners (Figure 2A,B). Further investigation of the signal molecules revealed that components of the proliferation- and survival-associated MAPK and PI3K/Akt pathways were markedly inhibited by AMAD (Figure 3A,B).

Akt/PKB, a serine/threonine kinase well-known as a pivotal survival factor in signal transduction pathways involved in cell growth, cell cycle progression, survival, migration, epithelial-mesenchymal transition and angiogenesis, is a possible target for anticancer drug induced apoptosis. Overexpression of Akt has been reported to be related to drug resistance,[33] and treatment with anticancer drugs such as CPT-11 and growth factor deprivation has been shown to suppress the activity of Akt, leading to loss of cell viability and increase of apoptosis.[34] The mechanism by which Akt protects cells from death is likely to be multifactorial since Akt directly phosphorylates several components of the cell-death machinery.[35] Intriguingly, the PI3K-Akt

signaling pathway regulates the cellular localization of BCRP,[36,37] a putative molecular marker of side population cell phenotype and cancer stem cells.[38] Imatinib (Gleevec) could attenuate its resistance via inhibition of BCR-ABL, leading to the decreased phosphorylation of Akt and subsequently reduced BCRP expression.[39] Furthermore, imatinib-mediated inactivation of Akt resulted in doxorubicin retention by regulating BCRP function.[40] In the present study, the data revealed that AMAD inhibited Akt phosphorylation at serine 473 without significantly affecting Akt protein levels; moreover, the activity of Akt kinase was markedly inhibited by AMAD, as shown by the dephosphorylation of its downstream FoxO1, mTOR and GSK-3α/β (Figure 3).

How may expression of Her2/*neu* protein be downregulated by AMAD? Two possible mechanisms may be involved. First, AMAD downregulated Her2/*neu* protein at the mRNA level; and second, lysosome or ubiquitin-proteasome pathway regulated the degradation of Her2/*neu* by AMAD. Interestingly, our data revealed that AMAD decreased Her2/*neu* protein expression independent of its mRNA level (Figure 2C,D). However, protein turnover assay revealed that the half-life of Her2/*neu* protein was significantly reduced by AMAD (Figure 4). These suggested that downregulation of Her2/*neu* by AMAD was primarily dependent on Her2/*neu* protein stability.

Heat shock protein 90 is a protein chaperone functioning to promote the maturation and conformational stabilization of a subset of cellular proteins important in transducing proliferative and survival signals, including protein kinases (e.g., Her2, Raf-1), steroid receptors (e.g., androgen receptor and estrogen receptor), transcription factors (e.g., Hif-1α) and a number of mutant oncoproteins (e.g., v-Src, mutant EGFR and mutant B-Raf).[41,42] Given the critical roles of Hsp90 clients in tumor growth and maintenance, inhibition of Hsp90 has emerged as a possible strategy for the treatment of advanced cancers.[42] Our data revealed that AMAD markedly impaired the binding of Hsp90 and Her2, effectively promoted Her2/*neu* ubiquitination and destroyed the plasma membrane location of Her2/*neu*. (Figure 5B−D, Supporting Information Figure S1A). Interestingly, AMAD could bind both Her2/*neu* and Hsp90 (Supporting Information Figure S1B,C). Additionally, pretreatment with the proteasome inhibitor MG132 but not lysosome inhibitor chloroquine blocked the depletion of Her2/*neu* protein by AMAD, indicating that blockade of Her2/*neu* binding of Hsp90 by AMAD decreased Her2/*neu* protein by promoting its degradation in the proteasome (Figure 5). Interestingly, RNA interference via siRNA is an effective approach to silencing target genes. In the present study, the data also showed that AMAD suppressed proliferation and induced apoptosis of Her2/*neu*-overexpressing Calu-3 cells, and combination of AMAD and Her2-targeted siRNA had a synergetic effect (Figure 6).

To understand the probable molecular mechanism of emodin AMAD in disrupting the Her2−HSP90 interaction, we have performed molecular docking studies. Our choice for docking emodin AMAD (comprising a benzoquinone ring structure) into both Her2 and HSP90 nucleotide binding sites was based on the following reasons: (a) emodin has been previously reported as a tyrosine kinase inhibitor,[27−31] (b) the benzoquinone ansamycin family of compounds block HSP90 chaperone activity through their interaction with the ATP-binding site of HSP90,[43] and (c) it is not clear from the present investigation whether emodin AMAD binds exclusively to Her2 or HSP90; however, the present data clearly suggested the disruption of the Her2−HSP90 interaction. With this backdrop, emodin AMAD was individually docked into the nucleotide binding sites of Her2 and HSP90. The computational data suggests that AMAD is able to bind to both proteins with comparable binding energies (Glide scores). In the context of HSP90 as the target for AMAD, we speculate that the activity of emodin AMAD is attributed to its interaction with the ATP-binding pocket of HSP90, resulting in remodeling of chaperone complexes and subsequent degradation of Her2. In the context of Her2 as the target for AMAD, we postulate that emodin AMAD binding to the ATP-binding pocket of Her2 may cause structural distortion of the glycine-rich P-loop, which, in turn, may allosterically affect the conformation of the adjacent Cα-helix and eventually impact the binding of HSP90 to Her2. It may be noted that the docking results presented here are not validated by site-directed mutagenesis or cocrystal complex of AMAD-Her2 and AMAD-HSP90; however, in the interim the binding model of AMAD may serve as a guide for further SAR optimization and reveal their potential target site.

In summary, we presented cell biological evidence that disruption of the PI3K/Akt-dependent pathway was involved in the inhibition of cell growth and induction of apoptosis in emodin AMAD treated Her2/*neu*-overexpressing cancer cells. Importantly, we demonstrated for the first time that emodin AMAD treatment led to blockade of Her2/*neu* binding to Hsp90, intracellular redistribution, enhanced ubiquitinylation and thus proteasomal degradation of Her2/*neu*, which may be represent as a novel approach for the targeted therapy of Her2/*neu*-overexpressing cancers.

■ ASSOCIATED CONTENT

Ⓢ Supporting Information. Tables of data for cytotoxicity of AMAD in diverse cell lines and the inhibition effect of AMAD on the growth of human non-small cell lung carcinoma (NSCLC) H460 cell xenograft in nude mice. Figures depicting AMAD depletion of the colocalization of Hsp90 and Her2/*neu* and binding to Hsp90 and Her2/*neu* and HPLC study of AMAD labeling by Cy7. This material is available free of charge via the Internet at http://pubs.acs.org.

■ AUTHOR INFORMATION

Corresponding Author

*Cancer Center, Sun Yat-sen University, 651 Dongfeng Road East, Guangzhou 510060, People's Republic of China. Tel: 86-20-87343163. Fax: 86-20-87343170. E-mail: fulw@mail.sysu.edu.cn.

■ ACKNOWLEDGMENT

This work was supported by the 863 Key Project Foundation of China (No. 2006AA09Z419); and the Natural Sciences Foundation of Guangdong province, China (No. 2008B030301331).

■ ABBREVIATIONS USED

AMAD, azide methyl anthraquinone derivative; ERK, extracellular signal-regulated kinase; FITC, fluorescein isothiocyanate; GAPDH, glyceraldehyde-3-phosphate dehydrogenase; Hsp90, heat shock protein 90; MAPK, mitogen-activated protein kinase; MTT, 3-(4,5-dimethylthiazol-2-y1)-2,5-diphenyltetrazolium bromide; PI, propidium iodide; PI3K, phosphatidylinositol 3-kinase; v/v, volume per volume

REFERENCES

(1) Slamon, D. J.; Godolphin, W.; Jones, L. A.; Holt, J. A.; Wong, S. G.; Keith, D. E.; Levin, W. J.; Stuart, S. G.; Udove, J.; Ullrich, A.; et al. Studies of the HER-2/neu proto-oncogene in human breast and ovarian cancer. *Science* **1989**, *244*, 707–712.

(2) Schraml, P.; Kononen, J.; Bubendorf, L.; Moch, H.; Bissig, H.; Nocito, A.; Mihatsch, M. J.; Kallioniemi, O. P.; Sauter, G. Tissue microarrays for gene amplification surveys in many different tumor types. *Clin. Cancer Res.* **1999**, *5*, 1966–1975.

(3) Agus, D. B.; Bunn, P. A.; Franklin, W.; Garcia, M.; Ozols, R. F. HER-2/neu as a therapeutic target in non-small cell lung cancer, prostate cancer, and ovarian cancer. *Semin. Oncol.* **2000**, *27*, 53−63, discussion 92−100.

(4) Nakamura, H.; Saji, H.; Ogata, A.; Hosaka, M.; Hagiwara, M.; Kawasaki, N.; Kato, H. Correlation between encoded protein overexpression and copy number of the HER2 gene with survival in non-small cell lung cancer. *Int. J. Cancer* **2003**, *103*, 61–66.

(5) Slamon, D. J.; Clark, G. M.; Wong, S. G.; Levin, W. J.; Ullrich, A.; McGuire, W. L. Human breast cancer: correlation of relapse and survival with amplification of the HER-2/neu oncogene. *Science* **1987**, *235*, 177–182.

(6) Fajac, A.; Benard, J.; Lhomme, C.; Rey, A.; Duvillard, P.; Rochard, F.; Bernaudin, J. F.; Riou, G. c-erbB2 gene amplification and protein expression in ovarian epithelial tumors: evaluation of their respective prognostic significance by multivariate analysis. *Int. J. Cancer* **1995**, *64*, 146–151.

(7) Menard, S.; Pupa, S. M.; Campiglio, M.; Tagliabue, E. Biologic and therapeutic role of HER2 in cancer. *Oncogene* **2003**, *22*, 6570–6578.

(8) Rowinsky, E. K. The erbB family: targets for therapeutic development against cancer and therapeutic strategies using monoclonal antibodies and tyrosine kinase inhibitors. *Annu. Rev. Med.* **2004**, *55*, 433–457.

(9) Krause, D. S.; Van Etten, R. A. Tyrosine kinases as targets for cancer therapy. *N. Engl. J. Med.* **2005**, *353*, 172–187.

(10) Mani, A.; Gelmann, E. P. The ubiquitin-proteasome pathway and its role in cancer. *J. Clin. Oncol.* **2005**, *23*, 4776–4789.

(11) Ciechanover, A. The ubiquitin-proteasome pathway: on protein death and cell life. *EMBO J.* **1998**, *17*, 7151–7160.

(12) Yan, Y.; Su, X.; Liang, Y.; Zhang, J.; Shi, C.; Lu, Y.; Gu, L.; Fu, L. Emodin azide methyl anthraquinone derivative triggers mitochondrial-dependent cell apoptosis involving in caspase-8-mediated Bid cleavage. *Mol. Cancer Ther.* **2008**, *7*, 1688–1697.

(13) Zheng, L. S.; Wang, F.; Li, Y. H.; Zhang, X.; Chen, L. M.; Liang, Y. J.; Dai, C. L.; Yan, Y. Y.; Tao, L. Y.; Mi, Y. J.; Yang, A. K.; To, K. K.; Fu, L. W. Vandetanib (Zactima, ZD6474) antagonizes ABCC1- and ABCG2-mediated multidrug resistance by inhibition of their transport function. *PLoS One* **2009**, *4*, e5172.

(14) Way, T. D.; Kao, M. C.; Lin, J. K. Apigenin induces apoptosis through proteasomal degradation of HER2/neu in HER2/neu-overexpressing breast cancer cells via the phosphatidylinositol 3-kinase/Akt-dependent pathway. *J. Biol. Chem.* **2004**, *279*, 4479–4489.

(15) Choudhury, A.; Charo, J.; Parapuram, S. K.; Hunt, R. C.; Hunt, D. M.; Seliger, B.; Kiessling, R. Small interfering RNA (siRNA) inhibits the expression of the Her2/neu gene, upregulates HLA class I and induces apoptosis of Her2/neu positive tumor cell lines. *Int. J. Cancer* **2004**, *108*, 71–77.

(16) Aertgeerts, K; S., R.; Yano, J; Sang, B. C.; Zou, H; Snell, G; Jennings, A; Iwamoto, K; Habuka, N; Hirokawa, A; Ishikawa, T; Tanaka, T; Miki, H; Ohta, Y; Sogabe, S. Structural Analysis of the Mechanism of Inhibition and Allosteric Activation of the Kinase Domain of HER2 Protein. *J. Biol. Chem.* **2011**, *286*, 18756–18765.

(17) Obermann, W. M.; S., H.; Russo, A. A.; Pavletich, N. P.; Hartl, F. U. In vivo function of Hsp90 is dependent on ATP binding and ATP hydrolysis. *J. Cell. Biol.* **1998**, *143*, 901–910.

(18) Marte, B. M.; Downward, J. PKB/Akt: connecting phosphoinositide 3-kinase to cell survival and beyond. *Trends Biochem. Sci.* **1997**, *22*, 355–358.

(19) Vanhaesebroeck, B.; Alessi, D. R. The PI3K-PDK1 connection: more than just a road to PKB. *Biochem. J.* **2000**, *346* (Part 3), 561–576.

(20) Jeong, J. H.; An, J. Y.; Kwon, Y. T.; Li, L. Y.; Lee, Y. J. Quercetin-induced ubiquitination and down-regulation of Her-2/neu. *J. Cell Biochem.* **2008**, *105*, 585–595.

(21) Xu, W.; Marcu, M.; Yuan, X.; Mimnaugh, E.; Patterson, C.; Neckers, L. Chaperone-dependent E3 ubiquitin ligase CHIP mediates a degradative pathway for c-ErbB2/Neu. *Proc. Natl. Acad. Sci. U.S.A.* **2002**, *99*, 12847–12852.

(22) Citri, A.; Alroy, I.; Lavi, S.; Rubin, C.; Xu, W.; Grammatikakis, N.; Patterson, C.; Neckers, L.; Fry, D. W.; Yarden, Y. Drug-induced ubiquitylation and degradation of ErbB receptor tyrosine kinases: implications for cancer therapy. *EMBO J.* **2002**, *21*, 2407–2417.

(23) Isaacs, J. S.; Xu, W.; Neckers, L. Heat shock protein 90 as a molecular target for cancer therapeutics. *Cancer Cell* **2003**, *3*, 213–217.

(24) Xu, W.; Mimnaugh, E.; Rosser, M. F.; Nicchitta, C.; Marcu, M.; Yarden, Y.; Neckers, L. Sensitivity of mature Erbb2 to geldanamycin is conferred by its kinase domain and is mediated by the chaperone protein Hsp90. *J. Biol. Chem.* **2001**, *276*, 3702–3708.

(25) Xu, W.; Mimnaugh, E. G.; Kim, J. S.; Trepel, J. B.; Neckers, L. M. Hsp90, not Grp94, regulates the intracellular trafficking and stability of nascent ErbB2. *Cell Stress Chaperones* **2002**, *7*, 91–96.

(26) Mimnaugh, E. G.; Chavany, C.; Neckers, L. Polyubiquitination and proteasomal degradation of the p185c-erbB-2 receptor protein-tyrosine kinase induced by geldanamycin. *J. Biol. Chem.* **1996**, *271*, 22796–22801.

(27) Zhang, L. L.; Y., K.; Xi, L.; Hong, R. L.; Kim, D. S.; Chen, C. F.; Hortobagyi, G. N.; Chang, C.; Hung, M. C. Tyrosine kinase inhibitors, emodin and its derivative repress HER-2/neu-induced cellular transformation and metastasis-associated properties. *Oncogene* **1998**, *16*, 2855–2863.

(28) Zhang, L.; Chang, C. J.; Bacus, S. S.; Hung, M. C. Suppressed transformation and induced differentiation of HER-2/neu-overexpressing breast cancer cells by emodin. *Cancer Res.* **1995**, *55*, 3890–3896.

(29) Zhang, L.; Hung, M. C. Sensitization of HER-2/neu-overexpressing non-small cell lung cancer cells to chemotherapeutic drugs by tyrosine kinase inhibitor emodin. *Oncogene* **1996**, *12*, 571–576.

(30) Su, Y. J.; Tsai, M. S.; Kuo, Y. H.; Chiu, Y. F.; Cheng, C. M.; Lin, S. T.; Lin, Y. W. Role of Rad51 downregulation and ERK1/2 inactivation in emodin and mitomycin C-induced synergistic cytotoxicity in human non-small cell lung cancer cells. *Mol. Pharmacol.* **2010**, *77*, 633–643.

(31) Zhang, L.; Lau, Y. K.; Xia, W.; Hortobagyi, G. N.; Hung, M. C. Tyrosine kinase inhibitor emodin suppresses growth of HER-2/neu-overexpressing breast cancer cells in athymic mice and sensitizes these cells to the inhibitory effect of paclitaxel. *Clin. Cancer Res.* **1999**, *5*, 343–353.

(32) Raja, S. M.; Clubb, R. J.; Bhattacharyya, M.; Dimri, M.; Cheng, H.; Pan, W.; Ortega-Cava, C.; Lakku-Reddi, A.; Naramura, M.; Band, V.; Band, H. A combination of Trastuzumab and 17-AAG induces enhanced ubiquitinylation and lysosomal pathway-dependent ErbB2 degradation and cytotoxicity in ErbB2-overexpressing breast cancer cells. *Cancer Biol. Ther.* **2008**, *7*, 1630–1640.

(33) Page, C.; Lin, H. J.; Jin, Y.; Castle, V. P.; Nunez, G.; Huang, M.; Lin, J. Overexpression of Akt/AKT can modulate chemotherapy-induced apoptosis. *Anticancer Res.* **2000**, *20*, 407–416.

(34) Nakashio, A.; Fujita, N.; Rokudai, S.; Sato, S.; Tsuruo, T. Prevention of phosphatidylinositol 3′-kinase-Akt survival signaling pathway during topotecan-induced apoptosis. *Cancer Res.* **2000**, *60*, 5303–5309.

(35) Vivanco, I.; Sawyers, C. L. The phosphatidylinositol 3-Kinase AKT pathway in human cancer. *Nat. Rev. Cancer* **2002**, *2*, 489–501.

(36) Mogi, M.; Yang, J.; Lambert, J. F.; Colvin, G. A.; Shiojima, I.; Skurk, C.; Summer, R.; Fine, A.; Quesenberry, P. J.; Walsh, K. Akt signaling regulates side population cell phenotype via Bcrp1 translocation. *J. Biol. Chem.* **2003**, *278*, 39068–39075.

(37) Bleau, A. M.; Hambardzumyan, D.; Ozawa, T.; Fomchenko, E. I.; Huse, J. T.; Brennan, C. W.; Holland, E. C. PTEN/PI3K/Akt pathway regulates the side population phenotype and ABCG2 activity in glioma tumor stem-like cells. *Cell Stem Cell* **2009**, *4*, 226–235.

(38) Dean, M.; Fojo, T.; Bates, S. Tumour stem cells and drug resistance. *Nat. Rev. Cancer* **2005**, *5*, 275–284.

(39) Nakanishi, T.; Shiozawa, K.; Hassel, B. A.; Ross, D. D. Complex interaction of BCRP/ABCG2 and imatinib in BCR-ABL-expressing cells: BCRP-mediated resistance to imatinib is attenuated by imatinib-induced reduction of BCRP expression. *Blood* **2006**, *108*, 678–684.

(40) Chu, T. S.; Chen, J. S.; Lopez, J. P.; Pardo, F. S.; Aguilera, J.; Ongkeko, W. M. Imatinib-mediated inactivation of Akt regulates ABCG2 function in head and neck squamous cell carcinoma. *Arch. Otolaryngol., Head Neck Surg.* **2008**, *134*, 979–984.

(41) Chandarlapaty, S.; Sawai, A.; Ye, Q.; Scott, A.; Silinski, M.; Huang, K.; Fadden, P.; Partdrige, J.; Hall, S.; Steed, P.; Norton, L.; Rosen, N.; Solit, D. B. SNX2112, a synthetic heat shock protein 90 inhibitor, has potent antitumor activity against HER kinase-dependent cancers. *Clin. Cancer Res.* **2008**, *14*, 240–248.

(42) Mitsiades, C. S.; Mitsiades, N. S.; McMullan, C. J.; Poulaki, V.; Kung, A. L.; Davies, F. E.; Morgan, G.; Akiyama, M.; Shringarpure, R.; Munshi, N. C.; Richardson, P. G.; Hideshima, T.; Chauhan, D.; Gu, X.; Bailey, C.; Joseph, M.; Libermann, T. A.; Rosen, N. S.; Anderson, K. C. Antimyeloma activity of heat shock protein-90 inhibition. *Blood* **2006**, *107*, 1092–1100.

(43) Whitesell, L; M., E.; De Costa, B; Myers, C. E.; Neckers, L. M. Inhibition of heat shock protein HSP90-pp60v-src heteroprotein complex formation by benzoquinone ansamycins: essential role for stress proteins in oncogenic transformation. *Proc. Natl. Acad. Sci. U.S.A.* **1994**, *91*, 8324–8328.